





# The Dielectric Constant of Sea Water and Extension to High Salinity

David M. Le Vine , *Life Fellow, IEEE*, Ming Li , *Member, IEEE*, Yiwen Zhou , *Member, IEEE*, Roger H. Lang , *Life Fellow, IEEE*, Emmanuel P. Dinnat , *Senior Member, IEEE*, Yan Soldo , and Paolo de Matthaëis , *Senior Member, IEEE*

**Abstract**—The range of salinity and temperature measurements used to develop models for the dielectric constant of sea water have in the past been limited to values appropriate for the open ocean. But there are important water bodies, such as the Great Salt Lake in Utah, with salinities much larger than those encountered in the open ocean. Extrapolating existing models to the values of salinity beyond the limits of the data used to create the model can result in unrealistic predictions in remote sensing applications. This can be prevented by using a model for conductivity based on the definition of salinity and ensuring that polynomials used to model the other unknown parameters result in bounded behavior at high salinity. New laboratory measurements with high salinity (up to 150 pss) are reported and used to test a model with these adjustments.

**Index Terms**—Dielectric constant, L-band, microwave remote sensing, ocean salinity.

## I. INTRODUCTION

THE accurate knowledge of the dielectric constant of sea water is important for remote sensing of surface parameters, such as sea surface temperature (SST) and sea surface salinity (SSS). With the advent of sensors in space, SMOS [1], Aquarius [2], and SMAP [3] are capable of measuring SSS, motivated modern measurements of the dielectric constant [4], [5] and the development of new models [5], [6] for the dielectric constant at L-band (1.4 GHz). In the past, the range of salinity included in the data used to create these models has been restricted to values typically encountered in the open ocean (e.g., less than 40 on the practical salinity scale, pss). However, there are many smaller

water bodies with much higher salinity. Notable examples are the Great Salt Lake in Utah with salinity on the order of 150 pss and Garabogazköl lagoon in Turkmenistan with even higher salinity. Unfortunately, existing models for the dielectric constant, based on the measurements limited to the modest values of salinity, cannot simply be extended to higher values of salinity. The problem is that the polynomials in salinity ( $S$ ) and temperature ( $T$ ) used to represent the unknown parameters in the models are not constrained outside the range of  $S$  and  $T$  used to determine their coefficients. While the models for the dielectric constant may be very good within that range, outside that range they can lead to unrealistic behavior.

Research is reported here to develop a model that represents the dielectric constant accurately for typical ocean water and behaves well at high salinity. Laboratory measurements made at 1.413 GHz [4], [5] are being repeated at 0.707 GHz ( $P$ -band) as a part of research to develop a model that applies over a wide bandwidth suitable for future remote sensing of salinity [8], [9], [10]. The focus of these measurements is  $S$  and  $T$  in the range applicable to the open ocean, but measurements at values of high salinity (50, 75, 100, and 150 pss) are included. Measurements at  $T = 20^\circ\text{C}$  have been made at these high values of salinity and will be compared here with a model recently modified to apply at high salinity [11].

## II. BACKGROUND

### A. Dielectric Constant

At frequencies near 1.4 GHz where remote sensing of SSS is currently being done (i.e., by SMAP and SMOS), contemporary models for the dielectric constant of sea water have the form [12]:

$$\epsilon_{sw} = \epsilon_{\infty}(S, T) + \frac{\epsilon_s(S, T) - \epsilon_{\infty}(S, T)}{1 + j\omega\tau_{sw}(S, T)} - \frac{j\sigma(S, T)}{\omega\epsilon_0} \quad (1)$$

where  $\omega = 2\pi f$  and  $\epsilon_0$  is the permittivity of free space. The conductivity  $\sigma$ , the relaxation time  $\tau_{sw}$ , and  $\epsilon_{\infty}$  and  $\epsilon_s$  are the parameters to be determined. In one of the first such models, Klein and Swift [7] set  $\epsilon_{\infty} = 4.9$ , used the fresh water ( $S = 0$ ) value for the relaxation time and fit the remaining unknowns  $\sigma$  and  $\epsilon_s$  to laboratory measurements at 1.4 and 2.7 GHz. This model worked well in the range of values represented by the measurements ( $5 < T < 30^\circ\text{C}$  and  $4 < S < 35$  pss [12]) and has been successfully used to retrieve SSS by SMOS [13]. However, because the polynomials used are not constrained outside of this

Manuscript received 28 August 2023; revised 18 January 2024; accepted 19 February 2024. Date of publication 23 February 2024; date of current version 11 March 2024. This work was supported by National Aeronautics and Space Administration under Grant NN17AK01G. (Corresponding author: David M. Le Vine.)

David M. Le Vine and Emmanuel P. Dinnat are with the Cryospheric Sciences Laboratory, NASA Goddard Space Flight Center, Greenbelt, MD 20771 USA (e-mail: david.m.levine@nasa.gov; emmanuel.dinnat@nasa.gov).

Ming Li and Roger H. Lang are with the Department of Electrical and Computer Engineering, The George Washington University, Washington, DC 20052 USA (e-mail: mingli@email.gwu.edu; lang@gwu.edu).

Yiwen Zhou is with the Swiss Federal Institute for Forest, Snow and Landscape Research (WSL), 8903 Birmensdorf, Switzerland (e-mail: yiwen.zhou920@wsl.ch).

Yan Soldo is with the European Space Agency (ESA/ESTEC), 2201 AZ Noordwijk, The Netherlands (e-mail: yan.soldo@esa.int).

Paolo de Matthaëis is with the Cryospheric Sciences Laboratory, NASA Goddard Space Flight Center, Greenbelt, MD 20771 USA, and also with the University of Maryland, Baltimore, MD 21250 USA (e-mail: paolo.dematthaëis@nasa.gov).

Digital Object Identifier 10.1109/JSTARS.2024.3369552

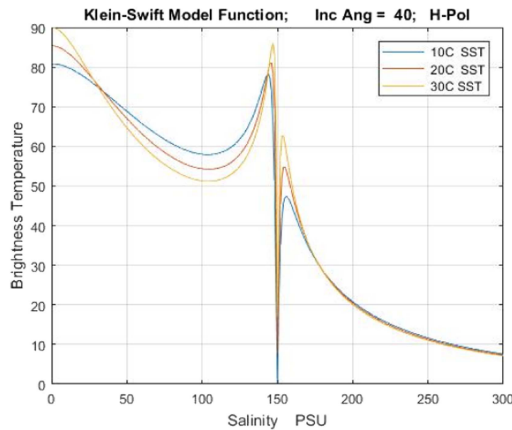


Fig. 1. Brightness temperature at  $40^\circ$  incidence and horizontal polarization for a flat-water surface as a function of salinity for  $T = 10, 20,$  and  $30^\circ\text{C}$ .

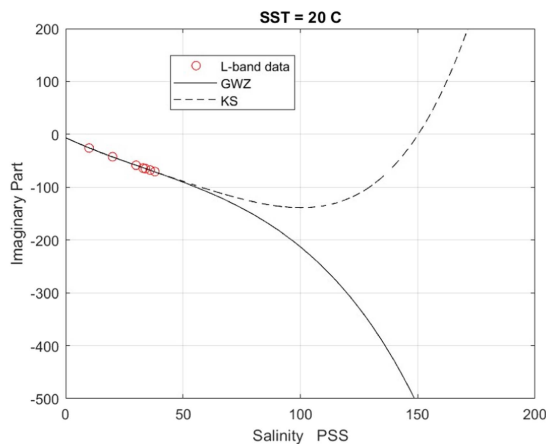


Fig. 2. Imaginary part of the models of Zhou et al. [5] labeled GWZ, and Klein and Swift [7] labeled KS, as a function of salinity at  $20^\circ\text{C}$ .

range, the model predicts unrealistic behavior at high salinity. This is illustrated in Fig. 1, which reports the H-pol brightness temperature predicted by this model as a function of  $S$  for an incidence angle of  $40^\circ$  and for several values of temperature. For  $S < 50$  pss, the brightness temperature TB behaves as one would expect, decreasing with increasing  $S$  and increasing with increased  $T$ . However, the extension to large  $S$  is marked by an obvious singularity at 150 pss. (Fig. 1 also indicates that the behavior of TB with temperature changes near  $S = 35$  pss. See Appendix D for a discussion.)

The singular behavior occurs because the polynomials used to model the parameters  $\sigma$ ,  $\tau_{sw}$ , and  $\varepsilon_s$  in (1) are not constrained to fit data outside of the range of the measurements. This is illustrated in Fig. 2, which shows the imaginary part of the dielectric constant [i.e., the imaginary part of (1)] as a function of salinity at  $20^\circ\text{C}$ . The imaginary part is shown for two models, the model of Klein and Swift [7] labeled KS in the figure and the more recent model of Zhou et al. [5], which is based on an extensive set of modern measurement of the dielectric constant at 1.4 GHz [4], [5]. The Zhou et al. [5] model, labeled GWZ

in Fig. 2, also uses polynomials in  $S$  and  $T$  to represent the parameters  $\sigma$ ,  $\tau_{sw}$ , and  $\varepsilon_s$ . The imaginary parts of these two models grow in quite different directions and without bound at large  $S$ . In addition, the imaginary part of the KS model changes sign at 150 pss, which is the mathematical reason for the singular behavior, as shown in Fig. 1.

Research is reported here to develop a model that performs well over the open ocean and also at high salinity and avoids problems, such as shown in Figs. 1 and 2. Two important changes have been adopted to achieve this goal.

- 1) Instead of representing the conductivity as a polynomial with coefficients determined as a part of fitting unknowns to the data, the modern definition of salinity given in terms of conductivity and temperature [14], [15] will be used. This was first proposed by Stogryn et al. [16], who inverted the equations for salinity as a function of conductivity and temperature, which comprise this definition to form an expression for  $\sigma(S, T)$ . The result is an expression for conductivity, which is essentially correct by definition (i.e., by the definition of salinity). This inversion was extended to include  $S < 2$  pss and is now available as an international standard [15], [17].
- 2) The parameters,  $\varepsilon_s(S, T)$  and  $\tau(S, T)$ , must reduce to the freshwater value when  $S = 0$ ; consequently, both should have the form [18]

$$\varepsilon_s(S, T) = \varepsilon_s(0, T) [1 + Sa(S, T)] \quad (2a)$$

$$\tau_{sw}(S, T) = \tau_{sw}(0, T) [1 + Sb(S, T)] \quad (2b)$$

where  $\varepsilon_s(0, T)$  and  $\tau_{sw}(0, T)$  are the freshwater values and  $a(S, T)$  and  $b(S, T)$  are to be determined from observations. In the modification being made here,  $a(S, T)$  and  $b(S, T)$  are represented by polynomials in  $S$  and  $T$  but with equal order in  $S$ , which prevents the unbounded behavior of the second term in (1) at large  $S$ .

A model with these modifications has been reported by Le Vine et al. [11]. It will be called GW2022 in the text to follow. The polynomials  $a(S, T)$  and  $b(S, T)$  in the GW2022 model have been fitted to the  $L$ -band data, as described in [5], and the conductivity  $\sigma(S, T)$  is given by McDougall et al. [17]. The GW2022 model fits the  $L$ -band data as well as the GWZ model by Zhou et al. [5], which is a careful fit to the data but uses a polynomial to represent the conductivity. At  $L$ -band, there is very little difference between GW2022 and GWZ over the range of  $S$  and  $T$  covered by the measurements [11].

The difference between the GW2022 and GWZ models is at high salinity where GW2022 is well behaved and GWZ is not (e.g., Fig. 2). However, until now, there has been no way to test the models against observation at high salinity. This changed when the research team at The George Washington University reported new measurements that included salinity of 50, 75, 100, and 150 pss [19].

### B. Measurements at P-Band

The focus of the measurement program at The George Washington University recently shifted from measurements at  $L$ -band [4], [5] to measurements at 0.707 GHz ( $P$ -band). The system



Fig. 3. Experimental setup for the measurement of the dielectric constant of sea water at  $P$ -band. The system is the same as used at  $L$ -band [4] except for the resonant cavity, which is larger and resonant at 0.707 GHz.

used to produce the measurements at  $L$ -band [4] has been modified to operate at  $P$ -band [19]. The goal of this work is to extend the range of validity of models used for the remote sensing of salinity by combining new measurements at  $P$ -band with the previous measurements at  $L$ -band to develop a model valid over a larger range of frequencies to support future wideband measurements of SSS [9], [10]. Although the focus is on  $S$  and  $T$  representative of the open ocean, provisions have been made to include measurements at 50, 75, 100, and 150 pss in the new  $P$ -band work.

Fig. 3 shows a photograph of the measurement system. It is identical to that used previously at  $L$ -band [4], [5] except for the resonant cavity (“ $P$ -band cavity”), which has been replaced with a larger cavity with resonance at 0.707 GHz [19]. The cavity is submerged in a distilled water/ethylene glycol solution, which is maintained at a given temperature by the “circulator.” Salt water enters the cavity through a quartz tube with an inner diameter of 0.2 mm and positioned along the axis of the cylindrical cavity. The change in resonant frequency and quality factor  $Q$  measured with the “network analyzer” are related to the dielectric constant of the water [4].

The new measurements at  $P$ -band at 35 pss are shown in Fig. 4. The figure reports the real part of the dielectric constant at the top and the imaginary part at the bottom both as a function of temperature for  $S = 35$  pss. The symbols represent the measurements. The solid curve in Fig. 4 is the prediction of the GWZ model. This model is fit to the measurements at  $L$ -band [5] but is evaluated here at  $P$ -band (0.707 GHz). This has been done primarily as a consistency check on the data. The model fits the data very well. Although evidence suggests that additional terms may be necessary at higher frequencies [12], [22], at frequencies lower than  $L$ -band, (1) remains a good representation and should be valid at  $P$ -band, at least at the resolution of the figures presented here. Also, the polynomial representing the conductivity in GWZ is very close to the definition [17] over this range of temperature and salinity at  $L$ -band (e.g., see Fig. 8

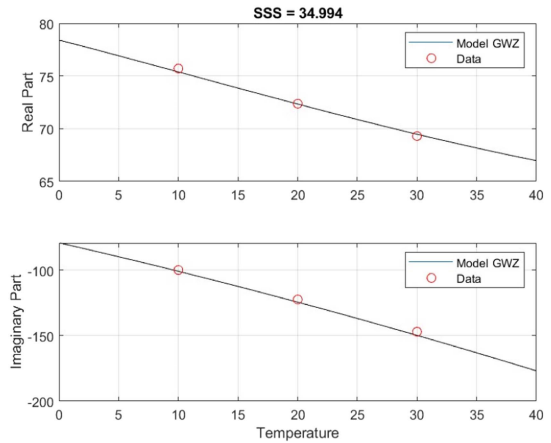


Fig. 4. Initial results of measurements at  $P$ -band (circles). The solid curve is the prediction of the GWZ model reported by Zhou et al. [5] but evaluated at the  $P$ -band.

in [11]). (See more about the relevance of the  $L$ -band models to  $P$ -band in the discussion in Section III).

### C. Measurements at High Salinity

In addition to the measurements as a function of temperature shown in Fig. 4, measurements were made at 20 °C as a function of salinity, including the values of salinity at 50, 75, 100, and 150 pss, which are well above the range included in the development of models, such as GWZ and that of Klein and Swift [7].

The sea water samples were provided by Ocean Scientific International, Ltd. For salinity less than 42 pss, standard procedure is to use a high-precision salinograph to determine the salinity samples (i.e., the accurate measure of the conductivity and conversion to pss using the definition of “practical salinity” [15]). However, because these samples are beyond the range of verified calibration, they were made by dilution, starting with a solution of high but unverified salinity and diluting the sample until the last sample was close to 35 pss. The last sample was measured with the salinograph and the salinity at the higher values was determined from the amount of dilution. This is the procedure endorsed by international standards [15].

The measurements at 20 °C are shown in Fig. 5. The real part of the dielectric constant is in the top panel and the imaginary part is shown in the bottom panel, plotted as a function of salinity. The symbols represent the measurements, and the solid black curve is the prediction of the GW2022 model. For comparison, the figure also includes the prediction of the GWZ model and model by Klein and Swift [7] labeled KS. The prediction of the three models is indistinguishable for  $S < 40$  but the predictions of the GWZ and KS models diverge rapidly from the data for  $S > 50$ . This is not a criticism of these models, which were based on the measurement’s representative of the open ocean (i.e.,  $S < 40$ ), but demonstrates the problem with extending such models to the larger values of salinity. In contrast, the GW2022 model, which has been modified, as described in Section II-A, to ensure bounded behavior at high salinity, also fits the measurements at higher salinity well.



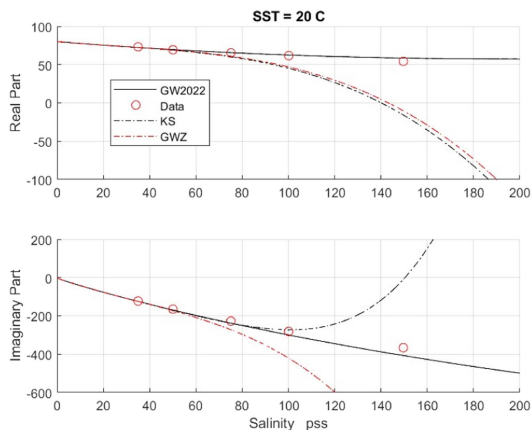


Fig. 5. Measurements at  $P$ -band (red circles) compared with model predictions. The solid line is the GW2022 model described in the text. The black dashed curve (KS) is the model of Klein and Swift [7], and the red dashed curve (GWZ) is the model by Zhou et al. [5] both of which use polynomials to fit model parameters to the data, including conductivity.

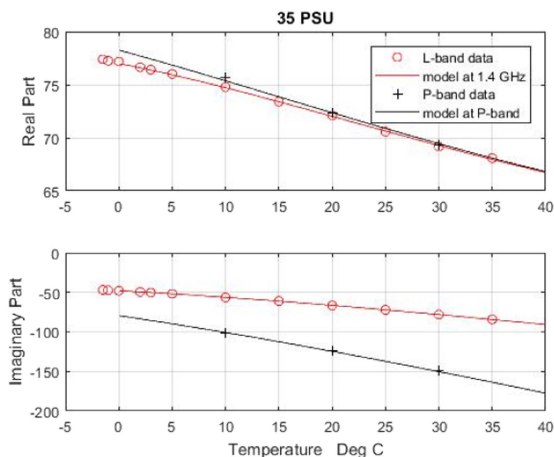


Fig. 6. Comparison of the GW2022 model with data at both  $P$ -band (“+”) and  $L$ -band ( $o$ ). The real part of the dielectric constant at the top and imaginary part on the bottom. This comparison is for  $S = 35$  pss.

### III. DISCUSSION

The objective of the measurements reported here is to test the GW2022 model [11] to see how well it applies at high values of salinity. The coefficients in the model were determined by fitting to data measured at  $L$ -band, and in an ideal case, the performance at high salinity would be made at  $L$ -band. Unfortunately, by the time the samples of sea water at high salinity arrived, the experimental equipment at GWU had already been converted to make measurements at  $P$ -band. However, it is reasonable to expect a model of the form of (1) to apply over a range of frequencies close to the frequency of the data used to determine its parameters, and this is especially true for lower frequencies where the form given in (1) is well established [12].

#### A. Relevance of Comparing at $P$ -Band

Experimental evidence justifying the use of the GW2022 model at  $P$ -band is given in Fig. 6. The figure shows a comparison of measurements at  $L$ -band and  $P$ -band with the model.

The top panel is the real part of the dielectric constant and the bottom panel shows the imaginary part, both plotted as a function of temperature for  $S = 35$  pss. In each panel, the data are given by the symbols and the solid line is the model prediction. The data at  $L$ -band ( $o$ ) are the measurements of [4] and [5], which were used to determine the model’s unknown parameters. The data at  $P$ -band (“+”) are the new data reported by Lang et al. [19] and shown in Fig. 4. The solid black curve is the GW2022 model evaluated at  $P$ -band and the solid red curve is the same model evaluated at  $L$ -band.

The model fits the data at both  $L$ -band and  $P$ -band very well. The consistent agreement over a range of frequencies is a consequence of the functional form of (1), which is based on solid physical arguments [18], [20], which apply at the low end of the microwave spectrum. At higher frequencies, additional resonant terms are needed [16], [21], [22], [23], [24], but at frequencies near 1.4 GHz, a model in the form of (1) with a conductivity term to account for current and a single term to account for the polarization of the water molecules has proven successful in remote sensing applications, such as measuring SSS [13], [25].

#### B. Issues

Fig. 5 shows that the GW2022 model behaves well at high salinity and is in reasonable agreement with the measurements. However, the agreement is not perfect. This is most evident at 150 pss where the model underpredicts the imaginary part and overpredicts the real part. In fact, there is some evidence of a trend with increasing salinity starting at about 100 pss. (See Appendix A, which shows the comparison with finer resolution.)

It is not clear from Fig. 5 that whether the departure of model and measurements at 150 pss is a measurement error or possibly the beginning of a trend due to a change in the true dependence of  $\sigma(S, T = 20)$  on salinity.

Measurement error cannot be ruled out. The measurement team at GWU has been very careful and followed procedures developed at  $L$ -band to ensure accuracy [4]. But measurements at such high salinity have not been made before. The measurement accuracy relies on a cavity with a high  $Q$  and the high loss at  $P$ -band at high salinity produces a lower  $Q$  than at  $L$ -band.

The equation for the conductivity as a function of salinity and temperature also could be an issue at high salinity. This equation is based on the definition of salinity in terms of conductivity [14]. The definition [14] and the inversion [17] to generate  $\sigma(S, T)$  were intended for use in the ocean and have not been verified for the large values of salinity.

At the large values of salinity, the dominant contribution to the imaginary part of the dielectric constant is the conductivity [i.e., the last term on the right in (1)]. The contribution of the polarization term is negligible in comparison (see Appendix B). Thus, the comparison of the imaginary part of the model with the measurements, as shown in Fig. 5, is essentially a comparison with measurements of the dependence of the conductivity  $\sigma(S, T)$ , as given in [17] on salinity. The relationship between conductivity and salinity given by [17] is approximately linear in salinity at large values of salinity (see Appendix C). But

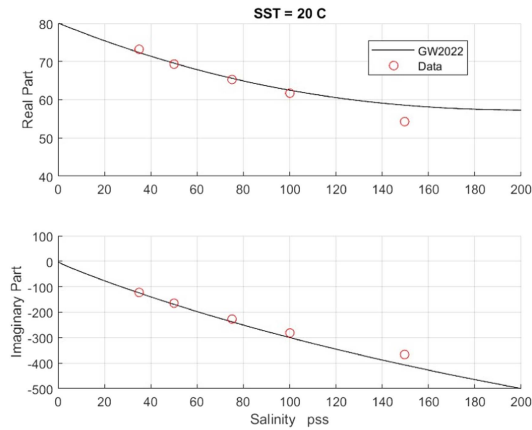


Fig. 7. Solid line is the GW2022 model prediction and the symbols ( $\circ$ ) are the  $P$ -band measurements. The top panel is the real part of the dielectric constant and the bottom panel is the imaginary part. The data are for  $T = 20^\circ\text{C}$ .

the saturation of the solution of salt and water would suggest there is an upper limit, and it is reasonable to expect this linear relationship to eventually change.

### C. Future Work

Additional measurements at a full range of temperatures are planned. This will help identify trends and possible measurement error. A measurement at even higher salinity will help define a trend if it exists.

## IV. CONCLUSION

The new measurements at  $P$ -band demonstrate that the adjustments made in the model for the dielectric constant, as described in Section II-A, and implemented in GW2022 result in a model that can apply over a large range of salinity from the full range over the ocean to the high salinity of water bodies, such as the Great Salt Lake in Utah. The measurements also demonstrate the danger of employing polynomials beyond their range of authenticity, and specifically, the danger of using polynomial-based models, such as [4], [5], and [7] beyond the range of salinity in the data used to generate the model.

However, the data are limited, and more work is needed to answer some important questions. Among these is whether the current relationship between salinity and conductivity, as given by McDougall et al. [17], is accurate at very high values of salinity.

More work is needed to confirm the behavior of the dielectric constant at high salinity and to determine if a model, such as GW2022 [11], is valid at all values of high salinity. It is anticipated that a measurement program to produce measurements over a full range of temperatures and salinity at the  $P$ -band will take place at The George Washington University [19] and that it will include the samples at 50, 75, 100, and 150 pss.

### APPENDIX A

Fig. 7 shows a comparison of the prediction of the GW2022 model [11] with the measurements at high salinity. The solid line is the GW2022 model and the ( $\circ$ ) represents the data.

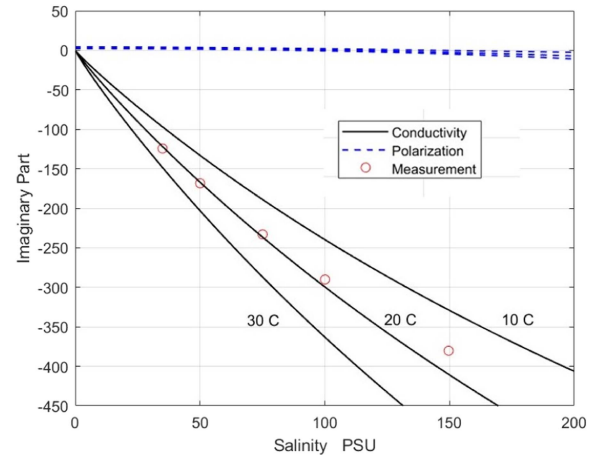


Fig. 8. Imaginary part of dielectric constant contributed by (solid line) the last term in (1) and by (dashed curve) the middle term in (1). The symbols  $\circ$  are the measurements. This example is for  $P$ -band,  $SST = 20^\circ\text{C}$  and was made using the GW2022 model.

The top panel is the real part and the bottom panel is the imaginary part of the dielectric constant. The data in Fig. 7 are the same as in Fig. 5 but presented here with more resolution to emphasize the difference between the model and measurement near 150 pss. There is also a small difference at 100 pss in both real and imaginary parts. Taken together, the differences between model and measurement at 100 and 150 pss suggest a possible systematic deviation of model and measurements for both real and imaginary parts that is increasing as a function of salinity.

### APPENDIX B

The imaginary part of the dielectric constant is the sum of two terms, the contribution from conductivity [the last term in (1)] and the contribution due to the polarization of the water molecule [second term in (1)]. Fig. 8 shows the contribution of these two terms as a function of salinity for several values of temperature. The contribution from conductivity is represented by the solid lines and the dashed lines (one for each temperature) represent the contribution from the polarization component of (1). The symbols represent the new  $P$ -band measurements.

Fig. 8 shows that the imaginary part of the dielectric constant is dominated by the conductivity term even at low values of salinity. The contribution from the polarization term (dashed) remains small compared with the conductivity term and varies relatively little over a wide range of  $S$  and  $T$ . The magnitude of the contribution of the conductivity term (solid line) varies significantly with temperature but is always much larger than the contribution of the polarization term.

At a fixed frequency, the only variable in the last term on the right in (1) is the conductivity  $\sigma(S, T)$ . Fig. 8 shows that the imaginary part of the dielectric constant is dominated by the conductivity term even at low values of salinity. Consequently, it is reasonable to assume that the behavior of plots, such as given in Figs. 5 and 6, that shows the imaginary part as a function of salinity at  $T = 20^\circ\text{C}$  is reflecting the behavior of the conductivity  $\sigma(S, T = 20)$  with varying salinity.

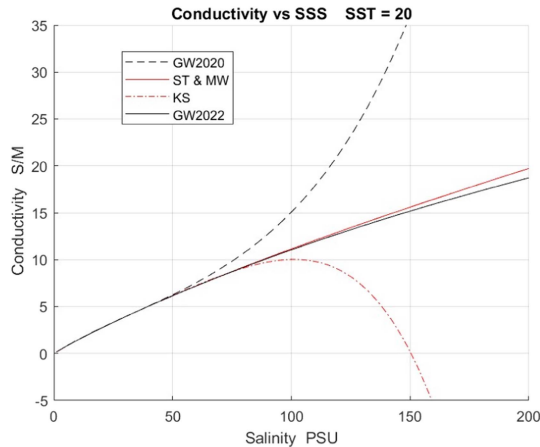


Fig. 9. Conductivity as a function of salinity for several different models. The solid black line is  $\sigma(S, T=20)$  from the definition of salinity, as given by McDougall et al. [17]. The red line is the version of this relationship derived by Stogryn et al. [16]. The red dashed line is the conductivity used in the model of Klein and Swift [7], and the black dashed line is the conductivity used in the GWZ model [5].

Fig. 8 also provides insight into why it is more difficult to measure salinity in cold water than in warm water. The change with salinity of the imaginary part of the dielectric constant is dominated by the conductivity, and it can be seen from Fig. 8 that the change with salinity of the conductivity term (slope of the solid line) decreases with temperature. It can also be seen from Fig. 6 that the change in the real part of the dielectric constant with a change in salinity is much less than that due to the imaginary part.

#### APPENDIX C

Fig. 9 shows a plot of the conductivity as a function of salinity for a temperature of 20 °C. The solid black line is  $\sigma(S, 20)$  from the definition of salinity, as given by McDougall et al. [17]. The red line is the original version of this relationship derived by Stogryn et al. [16] and used in the model by Meissner and Wentz [23], [24]. The dashed red line is the conductivity from the model by Klein and Swift [7] denoted by KS, and the dashed black line is the conductivity from the model by Zhou et al. [5] and called GWZ in the text of the article. In the KS and GWZ models, the conductivity is a polynomial determined by fitting to the data (i.e., laboratory measurements of the dielectric constant). The measurements are limited to 35 pss in the case of KS and 38 pss for GWZ [12]. Additional details about the models including the dependence of the conductivity with temperature can be found in [12].

Fig. 9 shows that all the models for conductivity are reasonably consistent for values of  $S < 40$  pss, but the polynomial-fitted models fail outside their region of validation. There is also a small difference between the version of the inversion derived by Stogryn et al. [16] represented by the (solid red line) and the version, which has been accepted internationally as the [15], [17].

The relationship between conductivity and salinity is nearly linear up to 150 pss. There is a slight curve downward at higher

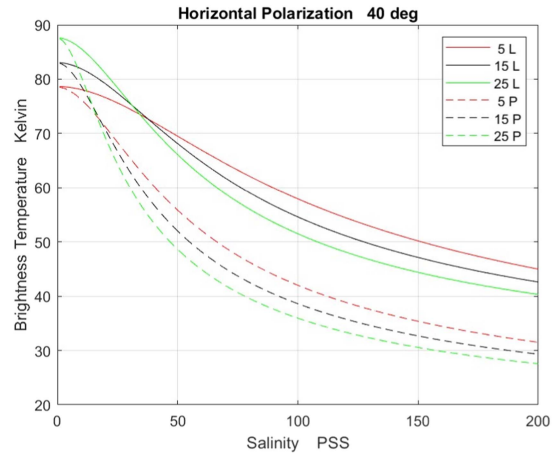


Fig. 10. Brightness temperature at horizontal polarization as a function of salinity and temperature for  $L$ -band (solid) and  $P$ -band (dashed). The examples are for  $T = 5$  °C (red line), 15 °C (black line), and 25 °C (green line).

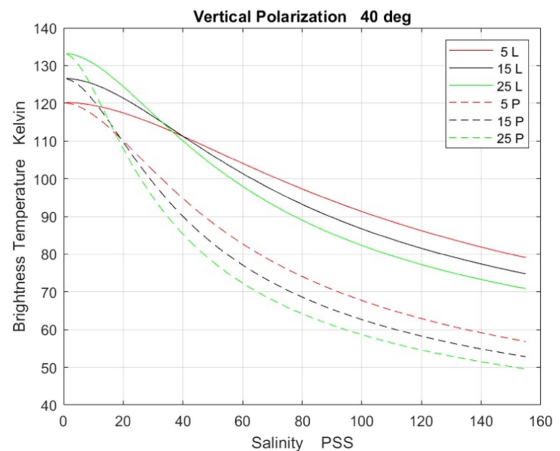


Fig. 11. Brightness temperature at vertical polarization as a function of salinity and temperature for  $L$ -band (solid) and  $P$ -band (dashed). The examples are for  $T = 5$  °C (red line), 15 °C (black line), and 25 °C (green line).

salinity. However, as mentioned in the text, this relationship has not been formally validated at such high values of salinity and the measurements reported here leave this question unresolved (e.g., see the discussion in Appendix A).

#### APPENDIX D

The objective of this article is to validate the GW2022 model for the dielectric constant of sea water for application to high salinity by comparing it with laboratory measurements. The modifications made to achieve such a model are described in Section II-A of this article and a comparison with the measurements is given in Figs. 5 and 6, which show that the model works well at both high salinity and salinity typical of the open ocean.

In Section III-A of the article, evidence is presented for using the GW2022 model at both  $L$ -band and  $P$ -band. Given this validation, it will be used in this appendix to discuss an important feature of emission from salt water that appears as the salinity is increased. This is illustrated in Figs. 10 and 11, which show the



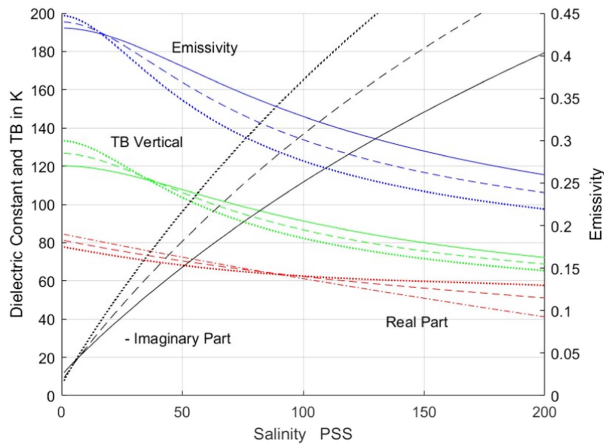


Fig. 12. Brightness temperature (left y-axis) and emissivity (right y-axis) at horizontal polarization and  $40^\circ$  incidence together with the real and imaginary part of the dielectric constant (left y-axis) as a function of salinity and temperature for  $L$ -band. These examples are for  $T = 5^\circ\text{C}$  (solid line),  $15^\circ\text{C}$  (dashed line), and  $25^\circ\text{C}$  (dotted line). The sign of the imaginary part of the dielectric constant has been changed to make a more compact figure.

brightness temperature TB of an ideal half-space of salt water as a function of temperature and salinity. The examples are for  $T = 5^\circ\text{C}$  (red line),  $15^\circ\text{C}$  (black line), and  $25^\circ\text{C}$  (green line). Fig. 10 is for horizontal polarization and Fig. 11 is for vertical polarization both at an incidence angle of  $40^\circ$ . The solid lines are for  $L$ -band (1.413 GHz) and the dashed lines are for  $P$ -band (0.707 GHz). A common feature of the curves is the decrease of TB as the salinity increases. This is because conductivity  $\sigma(S, T)$  in (1) increases monotonically as a function of  $S$  (e.g., see Fig. 8), and as the conductivity increases, the reflectivity  $R$  at the surface of the half-space becomes larger and the emissivity  $E = 1 - R$  decreases [9], [26]. That is, the half-space becomes more and more like an ideal perfect conductor, which has zero emission.

However, this decrease does not continue monotonically with temperature. Initially, for small  $S$ , the brightness temperature decreases with salinity but increases with  $T$ . This is as expected from the definition of emissivity,  $TB = E * T$ , where  $T$  is the physical temperature of the salt water. But as salinity increases, this dependence on  $T$  reverses. This happens between 35–40 pss for vertical polarization at  $L$ -band (solid lines) and near 20 pss at  $P$ -band (dashed lines), and at a little smaller  $S$  for horizontal polarization for both frequencies. For example, at vertical polarization and  $L$ -band, TB increases with  $T$  for  $S < 30$  pss, but for  $S > 40$  pss, TB decreases with an increase in  $T$ . The same is true for  $P$ -band but the transition region occurs earlier, near 18 pss, at vertical polarization.

The reason for this change in temperature dependence is the conductivity  $\sigma(S, T)$  in the last term in (1). This is illustrated in Fig. 12, which shows several parameters as a function of  $S$  and three values of  $T$ :  $T = 5^\circ\text{C}$  (solid line),  $15^\circ\text{C}$  (dashed line), and  $25^\circ\text{C}$  (dotted line). The imaginary part of the dielectric constant is shown in black and the real part in red. The imaginary part is dominated by the conductivity, as shown in Figs. 8 and 12 shows that for  $S > 50$  pss, the dielectric constant is dominated by the imaginary part. This is reflected in the behavior of the emissivity (blue curves), which decreases with increasing  $S$  and increasing

$T$ , both changes that result in an increase in conductivity. However, for  $S < 15$  pss, the real part dominates, and the influence of conductivity is not enough to overcome the natural (i.e.,  $S = 0$ ) tendency of the emissivity to increase with temperature. This is reflected in TB (green curves), which increases with an increase in temperature for low values of salinity. However, as  $S$  increases, the conductivity increases and, consequently, the magnitude of the imaginary part of the dielectric constant (black curves) also increases. Eventually, the temperature dependence of the imaginary part is sufficient to invert the freshwater behavior of the emissivity on  $T$  and overcome the direct dependence of TB on  $T$  (i.e.,  $TB = E * T$ ). At this point, the brightness temperature changes from increasing with temperature to decreasing with temperature.

The decrease in salinity and inversion of temperature dependence are more pronounced at  $P$ -band than at  $L$ -band (i.e., compare the solid and dashed curves in Figs. 10 and 11) because the lower frequency at  $P$ -band makes the conductivity term in (1) larger for a given value of salinity. But at very large values of salinity, the temperature dependence is the same at the two frequencies because the influence of conductivity dominates and the model for  $\sigma(S, T)$  is not frequency dependent.

## REFERENCES

- [1] S. Mecklenburg et al., "ESA's soil moisture and ocean salinity mission: Mission performance and operations," *IEEE Trans. Geosci. Remote Sens.*, vol. 50, no. 5, pp. 1354–1366, May 2012, doi: [10.1109/TGRS.2012.2187666](https://doi.org/10.1109/TGRS.2012.2187666).
- [2] D. M. Le Vine, G. S. E. Lagerloef, F. R. Colomb, S. H. Yueh, and F. A. Pellerano, "Aquarius: An instrument to monitor sea surface salinity from space," *IEEE Trans. Geosci. Remote Sens.*, vol. 45, no. 7, pp. 2040–2050, Jul. 2007, doi: [10.1109/TGRS.2007.898092](https://doi.org/10.1109/TGRS.2007.898092).
- [3] D. E. G. N. Entekhabi et al., "The soil moisture active and passive (SMAP) mission," *Proc. IEEE*, vol. 98, no. 5, pp. 704–716, May 2010.
- [4] R. H. Lang, Y. Zhou, C. Utku, and D. L. Vine, "Accurate measurements of the dielectric constant of seawater at  $L$  band," *Radio Sci.*, vol. 51, pp. 2–24, 2016, doi: [10.1002/2015RS005776](https://doi.org/10.1002/2015RS005776).
- [5] Y. Zhou, R. H. Lang, E. P. Dinnat, and D. M. Le Vine, "Seawater Debye model function at  $L$ -band and its impact on salinity retrieval from Aquarius," *IEEE Trans. Geosci. Remote Sens.*, vol. 59, no. 10, pp. 8103–8116, Oct. 2021, doi: [10.1109/TGRS.2020.3045771](https://doi.org/10.1109/TGRS.2020.3045771).
- [6] J. Boutin et al., "Correcting sea surface temperature spurious effects in salinity retrieved from spaceborne  $L$ -band radiometer measurements," *IEEE Trans. Geosci. Remote Sens.*, vol. 59, no. 9, pp. 7256–7269, Sep. 2021, doi: [10.1109/TGRS.2020.3030488](https://doi.org/10.1109/TGRS.2020.3030488).
- [7] L. Klein and C. Swift, "An improved model for the dielectric constant of seawater at microwave frequencies," *IEEE Trans. Antennas Propag.*, vol. 2, no. 1, pp. 104–111, Jan. 1977.
- [8] J. T. Johnson et al., "Microwave radiometry at frequencies from 500 to 1400 MHz: An emerging technology for Earth observations," *IEEE J. Sel. Topics Appl. Earth Observ. Remote Sens.*, vol. 14, pp. 4894–4914, 2021, doi: [10.1109/JSTARS.2021.3073286](https://doi.org/10.1109/JSTARS.2021.3073286).
- [9] D. M. Le Vine and E. P. Dinnat, "The multifrequency future for remote sensing of sea surface salinity from space," *Remote Sens.*, vol. 12, no. 9, Apr. 2020, Art. no. 1381, doi: [10.3390/rs12091381](https://doi.org/10.3390/rs12091381).
- [10] N. Vinogradova et al., "Satellite salinity observing system: Recent discoveries and the way forward," *Front. Mar. Sci.*, vol. 6, 2019, Art. no. 243, doi: [10.3389/fmars.2019.00243](https://doi.org/10.3389/fmars.2019.00243).
- [11] D. M. Le Vine, Y. Zhou, and R. H. Lang, "Model for dielectric constant of seawater based on  $L$ -band measurements with conductivity by definition," *IEEE Geosci. Remote Sens. Lett.*, vol. 19, 2022, Art. no. 1506605, doi: [10.1109/LGRS.2022.3221888](https://doi.org/10.1109/LGRS.2022.3221888).
- [12] S. M. Le Vine, R. H. Lang, Y. Zhou, E. P. Dinnat, and T. Meissner, "Status of the dielectric constant of sea water at  $L$ -band for remote sensing of salinity," *IEEE Trans. Geosci. Remote Sens.*, vol. 60, 2022, Art. no. 4210114, doi: [10.1109/TGRS.2022.3207944](https://doi.org/10.1109/TGRS.2022.3207944).

- [13] E. P. Dinnat, D. M. Le Vine, J. Boutin, T. Meissner, and G. Lagerloef, "Remote sensing of sea surface salinity: Comparison of satellite and in situ observations and impact of retrieval parameters," *Remote Sens.*, vol. 11, no. 7, 2019, Art. no. 750, doi: [10.3390/rs11070750](https://doi.org/10.3390/rs11070750).
- [14] E. L. Lewis, "The practical salinity scale 1978 and its antecedents," *IEEE J. Ocean. Eng.*, vol. 5, no. 1, pp. 3–8, Jan. 1980.
- [15] TEOS-10: IOC, SCOR, IAPSO, "The international thermodynamic equation of seawater–2010: Calculation and use of thermodynamic properties," Intergov. Oceanogr. Commission, Manuals and Guides No. 56, UNESCO (English), Paris, France, 2010.
- [16] A. Stogryn, H. T. Bull, K. Rubayi, and S. Iravanchy, "The microwave permittivity of sea and fresh water," Tech. Rep. 1995, Aerojet Gen. Corp., Azusa, CA, USA, 1995.
- [17] T. McDougall, P. Barker, and R. Pawlowicz, [help@teos-10.org], Version 3.05, Jan. 27, 2015.
- [18] R. Somaraju and J. Trumpf, "Frequency, temperature and salinity variation of the permittivity of seawater," *IEEE Trans. Antennas Propag.*, vol. 54, no. 11, pp. 3441–3448, Nov. 2006.
- [19] R. H. Lang, M. Li, B. O'Dell, Y. Zhou, and D. Le Vine, "Measurement of the dielectric constant of seawater at P band," in *Proc. IEEE Int. Geosci. Remote Sens. Symp.*, Kuala Lumpur, Malaysia, 2023, pp. 6978–6981.
- [20] P. J. W. Debye, *Polar Molecules*. New York, NY, USA: Dover, 1929.
- [21] H. J. Liebe, G. A. Hufford, and T. Manabe, "A model for the complex permittivity of water at frequencies below 1 THz," *Int. J. Infrared Millimeter Waves*, vol. 12, no. 7, pp. 659–675, Jan. 1991.
- [22] P. Rosenkranz, "A model for the complex dielectric constant of supercooled liquid water at microwave frequencies," *IEEE Trans. Geosci. Remote Sens.*, vol. 53, no. 3, pp. 1387–1393, Mar. 2015.
- [23] T. Meissner and F. Wentz, "The complex dielectric constant of pure and sea water from microwave satellite observations," *IEEE Trans. Geosci. Remote Sens.*, vol. 42, no. 9, pp. 1836–1849, Sep. 2004.
- [24] T. Meissner and F. Wentz, "The emissivity of the ocean surface between 6 and 90 GHz over a large range of wind speeds and Earth incident angles," *IEEE Trans. Geosci. Remote Sens.*, vol. 50, no. 8, pp. 3004–3026, Aug. 2012.
- [25] H. Kao, G. Lagerloef, T. Lee, O. Melnichenko, T. Meissner, and P. Hacker, "Assessment of Aquarius sea surface salinity," *Remote Sens.*, vol. 10, no. 9, 2018, Art. no. 1341, doi: [10.3390/rs10091341](https://doi.org/10.3390/rs10091341).
- [26] W. Peake, "Interaction of electromagnetic waves with some natural surfaces," *IRE Trans. Antennas Propag.*, vol. 7, no. 5, pp. 324–329, Dec. 1959.



**David M. Le Vine** (Life Fellow, IEEE) received the Ph.D. degree in electrical engineering from the University of Michigan, Ann Arbor, MI, USA.

His background is in electrical engineering with a specialization in electromagnetic theory and physics. He does his research with Earth Sciences Division, National Aeronautics and Space Administration (NASA) Goddard Space Flight Center, Greenbelt, MD, USA, where he works to develop techniques for microwave remote sensing of the environment from space. His focus is on passive remote sensing at the

long wavelength end of the microwave spectrum (e.g., *L*-band) with applications to remote sensing of soil moisture and sea surface salinity (SSS). Examples of this work are the development of the synthetic aperture radiometer, ESTAR, and the launch of AQUARIUS, a NASA Earth System Science Pathfinder mission to measure SSS. His teaching experience includes the Department of Electrical Engineering, University of Maryland, College Park, MD, USA, and an Adjunct Faculty with The George Washington University, Washington, DC, USA.

Dr. Le Vine was a Deputy Principal Investigator of AQUARIUS. He is a member of Ocean Salinity Science Team, which continues research on remote sensing of SSS. He is also a member of the science team for NASAs Soil Moisture Active Passive mission and the Quality Working Group supporting the European Space Agency Soil Moisture and Ocean Salinity mission. He has served on the Geoscience and Remote Sensing Society (GRSS) AdCom and several IEEE committees focused on engineering accreditation. He is a member of the GRSS, Antennas and Propagation Society, the International Union of Radio Science, and American Geophysical Union. He was a recipient of the IEEE/GRSS Distinguished Achievement Award in 2016 and the Golden Florin Award in 2014, for contributions to microwave radiometry.



**Ming Li** (Member, IEEE) received the B.S. degree in electronic information engineering from the Taiyuan University of Technology, Taiyuan, China, in 2016, and the Ph.D. degree in microwave testing technology and remote sensing from the University of Electronic Science and Technology of China, Chengdu, China, in 2021.

She is currently a Postdoctor with the Department of Electronic Computer and Engineering, The George Washington University, Washington, DC, USA. Her research fields include modeling bistatic radar scattering from multilayered random rough surface, remote sensing of soil moisture and temperature at root zone, and measurement of dielectric constant of soil and sea water.



**Yiwen Zhou** (Member IEEE) received the B.S. degree from Southeast University, Nanjing, China, in 2010, and the M.S. and Ph.D. degrees from The George Washington University (GWU), Washington, DC, USA, in 2012 and 2017, respectively, all in electrical engineering.

He was a Postdoctoral Scientist and a Lecturer with GWU with research topics focusing on active remote sensing of vegetation canopies and passive remote sensing of ocean salinity. He was a Research Scientist with Lincoln Agritech, Ltd., Lincoln University,

Christchurch, New Zealand. He is currently a Scientist with the Swiss Federal Institute for Forest, Snow and Landscape Research (WSL), Zürich, Switzerland, working on remote sensing of vegetation dynamics and soil moisture. His research interests include microwave dielectric measurements and sensor design, and emission and scattering model development and implementation in remote sensing of environment.

Dr. Zhou was a recipient of the URSI Young Scientist Award in 2021 and the IEEE Industrial Engineering Paper Award on Antenna Measurements and Applications in 2022. He is a member of IEEE GRSS and a senior member of URSI.



**Roger H. Lang** (Life Fellow, IEEE) received the B.S. and M.S. degrees in electrical engineering and the Ph.D. degree in electrophysics from the Polytechnic Institute of Brooklyn, New York, NY, USA, in 1962, 1964, and 1968, respectively.

He did his Postdoctoral Research in random media under Joe Keller with the Courant Institute of Mathematical Sciences, New York University, New York, NY, USA. He is currently an L. Stanley Crane Professor of engineering and applied science with The George Washington University, Washington, DC,

USA. He is known for the early development of the discrete scattering model for vegetation. More recently, he has been involved in remote sensing of sea water salinity and soil moisture under vegetation. His research interests include microwave remote sensing, electromagnetic wave propagation, and dielectric measurements.

Dr. Lang was a recipient of the Distinguished Achievement Award from the IEEE Geoscience and Remote Sensing Society. He is an active participant in the IEEE Geoscience and Remote Sensing Society. He was an Associate Editor for *Microwave Scattering and Propagation* and the co-Chair of the Technical Program Committee for the IGARSS'90 meeting held at College Park, MD, USA, in 1990. He was the Chair of the International URSI Commission F and is a member of the Editorial Board of *Waves in Random and Complex Media*.





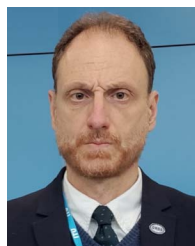
**Emmanuel P. Dinnat** (Senior Member, IEEE) received the advanced studies degree in instrumental methods in astrophysics and spatial applications and the Ph.D. degree in computer science, telecommunications, and electronics from the University Pierre and Marie Curie, Paris, France, in 1999 and 2003, respectively.

He is a Research Scientist with Cryospheric Sciences Laboratory, NASA Goddard Space Flight Center, Greenbelt, MD, USA. He has been working on the calibration, retrieval algorithm development, and science product validation for various airborne experiments and satellite missions. His research interests include active and passive microwave remote sensing, sea surface salinity, scattering from rough surfaces, atmospheric radiative transfer, and numerical simulations. His latest research focuses on high-latitude oceanography and the interactions between the cryosphere and oceans.



**Yan Soldo** received dual master's degree in aerospace engineering from Politecnico di Torino, Turin, Italy, and Supaéro-ISAE, Toulouse, France, in 2010, and the Ph.D. degree in remote sensing, with focus on SMOS mission, from CNES, Toulouse, France, in 2013.

He works in frequency management as the Earth Observation Directorate of ESA. There, he supports all ESA EO microwave missions in matters related to radio-frequency interference (RFI) and frequency management. He was previously a Scientist with Earth Sciences Division, NASA's Goddard Space Flight Center, Greenbelt, where he supported the SMAP and Aquarius missions, mostly on RFI topics.



**Paolo de Matthaëis** (Senior Member, IEEE) received the Laurea degree (*summa cum laude*) from the University of Rome "Tor Vergata," Rome, Italy, and the D.Sc. degree from George Washington University, Washington, DC, USA, in 1991 and 2005, respectively, both in electrical engineering.

After graduation, he was with European Space Agency, ESTEC, Noordwijk, The Netherlands, under the Young Graduate Trainee Program, and then with Remote Sensing Laboratory, University of Rome "Tor Vergata." He started working as a Research Associate with the NASA Goddard Space Flight Center, Greenbelt, MD, USA, where he is currently a Senior Research Engineer. His research interests include active and passive microwave remote sensing, with a focus on electromagnetic modeling of vegetation, land, and sea surface, and detection and mitigation of radio frequency interference. He was a part of the Science Algorithms Calibration/Validation team for the Aquarius instrument and is now a part of the team working on sea surface salinity estimation using SMAP.

Dr. de Matthaëis is a member of the U.S. National Committee for International Union of Radio Science (URSI), Gent, Belgium. He is a member of the IEEE Geoscience and Remote Sensing Society and has been active in the Frequency Allocations in Remote Sensing Technical Committee (FARS-TC). He is currently the Chair of the FARS-TC and has been the Chair or co-Chair since 2017.